



Review

Recent Development of Nickel-Rich and Cobalt-Free Cathode Materials for Lithium-Ion Batteries

Lukman Noerochim ^{1,*}, Suwarno Suwarno ^{2,*}, Nurul Hayati Idris ³ and Hermawan K. Dipojono ⁴

¹ Department of Materials and Metallurgical Engineering, Sepuluh Nopember Institute of Technology (ITS), Surabaya 60111, Indonesia

² Department of Mechanical Engineering, Sepuluh Nopember Institute of Technology (ITS), Surabaya 60111, Indonesia

³ Energy Storage Research Group, Faculty of Ocean Engineering Technology and Informatics, Universiti Malaysia Terengganu, Kuala Terengganu 21030, Malaysia; nurulhayati@umt.edu.my

⁴ Department of Engineering Physics, Institute of Technology Bandung (ITB), Bandung 40132, Indonesia; dipojono@tf.itb.ac.id

* Correspondence: lukman@mat-eng.its.ac.id (L.N.); warno@me.its.ac.id (S.S.)

Abstract: The exponential growth in the production of electric vehicles requires an increasing supply of low-cost, high-performance lithium-ion batteries. The increased production of lithium-ion batteries raises concerns over the availability of raw materials, especially cobalt for batteries with nickel-rich cathodes, in which these constraints can impact the high price of cobalt. The reliance on cobalt in these cathodes is worrisome because it is a high-cost, rare material, with an unstable supply chain. This review describes the need and feasibility of developing cobalt-free high-nickel cathode materials for lithium-ion batteries. The new type of cathode material, $\text{LiNi}_{1-x-y}\text{Mn}_x\text{Al}_y\text{O}_2$ promises a completely cobalt-free composition with almost the same electrochemical performance as that of the conventional high-nickel cathode. Therefore, this new type of cathode needs further research for its commercial applications.



Citation: Noerochim, L.; Suwarno, S.; Idris, N.H.; Dipojono, H.K. Recent Development of Nickel-Rich and Cobalt-Free Cathode Materials for Lithium-Ion Batteries. *Batteries* **2021**, *7*, 84. <https://doi.org/10.3390/batteries7040084>

Academic Editor: Catia Arbizzani

Received: 16 September 2021

Accepted: 21 November 2021

Published: 10 December 2021

Publisher's Note: MDPI stays neutral with regard to jurisdictional claims in published maps and institutional affiliations.



Copyright: © 2021 by the authors. Licensee MDPI, Basel, Switzerland. This article is an open access article distributed under the terms and conditions of the Creative Commons Attribution (CC BY) license (<https://creativecommons.org/licenses/by/4.0/>).

1. Introduction

The current global trend in the lithium-ion battery (LIB) industry is no longer monopolized by mobile gadgets and portable electronics applications but has undergone a significant shift toward the automotive industry, primarily due to transportation electrification. Lithium-ion batteries' market share has been growing for hybrid and fully electric vehicles (EV) over the last decade, showing a relatively rapid rise, which is estimated to reach 20% [1]. The rapid growth of electric car sales is driven by several factors, including incentives from the government and an increase in supporting infrastructure, such as the number of charging stations. In addition, the factor of lowering production costs and mature technology from the LIB fabrication process also boosted the percentage of EV vehicles. Meanwhile, the market response to EV-LIB vehicles seems to include four aspects, namely (1) efforts to reduce battery production costs, which are almost 50% of all EV production costs, so that EVs can compete with conventional vehicles or internal combustion engines (ICE), (2) the single-charge distance factor of EVs, (3) safety, and (4) increased power [2]. This has prompted researchers and industries around the world to compete to develop batteries with a higher energy density but with lower production costs.

Cobalt is the main element of LIB oxide layered cathodes, LiCoO_2 , since its commercialization in the 1990s by Sony in Japan and has become a successful product for powering electronic devices. On the other hand, the isostructural compound, LiNiO_2 (LNO), which is composed of low-cost and abundant Ni, has a significant change in properties during insertion/delithiation [3–5]. The LiNiO_2 has several phases during delithiation, and the

possibility of anion exchange with nickel makes maintaining its structural stability challenging [6,7]. Most work on LiNiO_2 in the past decade has been devoted to understanding the phase structural change by doping and substitution. Nevertheless, the commercialized layered-cathode today has its origin in LiCoO_2 . Replacing Co with Ni is one of the most reasonable choices. Other elements, such as Al and Mg, have also been shown to be good candidates for replacing Co [8,9]. Thus, the ongoing research on Co-free or high-Ni cathode is fundamentally aligned with the study on the modification of LiNiO_2 .

The two types of cathodes that are often used for the consumption of electric vehicles today are dominated first by $\text{LiNi}_{1-x-y}\text{Co}_x\text{Al}_y\text{O}_2$, in which $x + y < 0.2$ is referred to as NCA, and second by $\text{LiNi}_x\text{Mn}_y\text{Co}_z\text{O}_2$, in which $x + y + z = 1$ is referred to as NMC [10]. It is expected that the level of commercialization and production of these cathode materials will continue to rise for LIB over the next few decades. One concern that arises is the scarcity of the required mining materials that may be caused by large-scale LIB production. It is estimated that almost 50–80% of the total LIB production costs are spent on the purchase of materials for the manufacture of electrodes, especially cathode materials [11,12]. Due to the huge demands and needs of the market, the LIB production cost process continues to decline substantially, the battery cell size fabrication changes to a larger size format, and the mature battery production technology does not reduce the supply costs for electrode raw materials [13].

Concerns arise about the supply chain for the source of cobalt raw materials needed for LIB production, especially for the high-energy LIB type that uses NCA and NMC cathode materials. A cobalt supply deficit is forecasted early in 2030 [14]. Cobalt is a rare metal that has an important role in LIB. In addition, cobalt is also an important component in the manufacturing process of catalysts, semiconductors, magnetic recording devices, and a variety of high-strength metal alloys. This causes cobalt to be scarce and requires high costs in the extraction process because most of the cobalt comes from a byproduct with a low concentration of nickel and copper mining. Because 50% of world mine production in 2018 originated from copper-cobalt ore in the Democratic Republic of the Congo (DRC), where geopolitical instability and harsh working conditions could halt cobalt exports, cobalt is considered the most vulnerable source of feedstock [14].

In addition, China is currently the major producer, supplier, and consumer of cobalt in the world. Figure 1 shows a tremendous increase in China's import of ore and hydrometallurgy intermediate from the DRC since 2000 and 2005 [15]. China also expands its foreign ownership share for global mine production of cobalt from 11% to 33% of intermediate production capacity, including in the DRC. China is also predicted to have a deficit of cobalt supply by 2030 [16]. Cobalt production in China will be focused on meeting the needs of their domestic producers. The global dependence on cobalt can lead to high competition and conflicts. This will encourage the world to compete to produce cobalt-free cathodes for lithium-ion batteries [17].

Driven by the problem of cobalt supply, much research has been focused on reducing the amount of cobalt or completely removing Co from the composition to have a Co-free cathode. Current results, which are almost comparable with some commercial cathodes, are promising. This review describes the recent development of high-Ni and Co-free electrodes, which includes a discussion of the role of cobalt, strategies to reduce cobalt composition by doping, modification of the particle size, and synthesis engineering. The present work focuses on the significant development of the topics. The objective is to outline and fill the gap in the current development of Ni-rich cathode research. There are some existing reviews on these topics already, and this review is aimed to complement them [6,10].

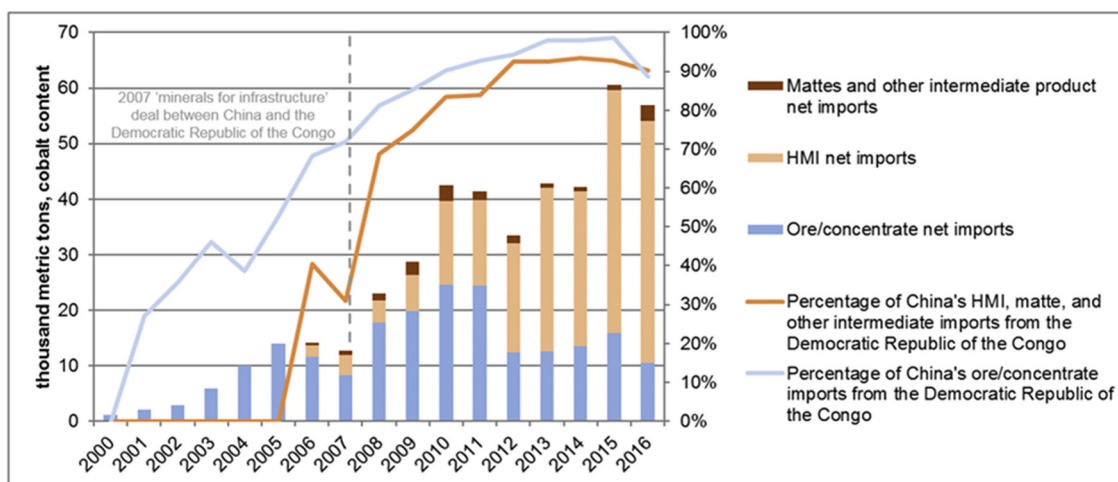


Figure 1. Percentage of cobalt content imported from the Democratic Republic of the Congo. HMI is referred to as hydrometallurgy intermediate [15].

2. The Role of Cobalt in LIBs

High-nickel cathodes are typically layered-mixed transition metal oxide structures and are frequently used to meet high-energy EV requirements. Among several NMC compositions, $\text{LiNi}_{1/3}\text{Mn}_{1/3}\text{Co}_{1/3}\text{O}_2$ (NMC111) has the highest electrochemical performance and safety [18]. The role of the Mn^{4+} ion in this composition is passive and only helps to maintain thermal stability, while the Co^{3+} ion helps increase the electronic conductivity and prevents interactions between Ni^{2+} and Li^+ [19–22]. The addition of Co for the partial substitution of Ni in the NMC cathode is beneficial for obtaining facile electron transfers because of the overlap of O 2p orbitals with $\text{Co}^{3+/4+}$ redox pairs for enhancing the electronic conductivity and leading to enhanced battery capacity [23–25]. Cation mixing $\text{Li}^+/\text{Ni}^{2+}$ in the Li layer will result in the formation of inactive $\text{Li}_2\text{Ni}_8\text{O}_{10}$, which inhibits the Li diffusion process, causing low power capability [26]. The I_{003}/I_{104} peak ratio (Figure 2a) shows a measure of the degree of cation mixing of $\text{Li}^+/\text{Ni}^{2+}$, in which a value higher than 1.2 indicates that the well-formed layered structure is more dominant than the small-degree cubic rock-salt Ni^{2+}O structure as a result of the cation mixing $\text{Li}^+/\text{Ni}^{2+}$ [27,28]. Partial Co substitution is very effective in preventing metal layer transitions due to cation mixing $\text{Li}^+/\text{Ni}^{2+}$. Multiphase transitions often occur in LNO-based materials, such as in the case of changes in “M + H2” and “H2 + H3” at voltages exceeding 4.0 V, which cause irreversible capacity [24]. Intensity peaks of the “M + H2” and “H2 + H3” transition are successfully reduced when Co is added (Figure 2b), which could be attributed to the partial replacement of the Ni^{2+} by $\text{Co}^{3+/4+}$ to reduce the cation mixing $\text{Li}^+/\text{Ni}^{2+}$. However, there has been no detailed explanation of this mechanism until now, so it still needs further investigation. The battery capacity mainly depends on the redox pairs $\text{Ni}^{2+}/\text{Ni}^{4+}$ and $\text{Co}^{3+}/\text{Co}^{4+}$ when operating at high voltages. Due to market demands related to the increased energy density and concerns about the dependence on cobalt, the next development, NMC111 was replaced by NMC622 $\text{LiNi}_{0.6}\text{Mn}_{0.2}\text{Co}_{0.2}\text{O}_2$ and NMC811 $\text{LiNi}_{0.8}\text{Mn}_{0.1}\text{Co}_{0.1}\text{O}_2$ with capacities of 180 mAh g^{-1} and 200 mAh g^{-1} , respectively [29]. Consequently, the nickel content increases, and as a result, there is a decrease in the cycle ability and thermal stability [18]. In addition, the de-lithiation process induces a drastic change in the volume of the crystal lattice which results in the cracking of the particles of the active material [30]. Moreover, the increase in the nickel composition of the NMC cathode will cause increased sensitivity to moisture, more mixing of $\text{Li}^+/\text{Ni}^{2+}$ cations, side reactions from electrolytes due to the presence of Ni^{4+} , and phase changes from spinel to rock salt structures due to the evolution of oxygen, especially at high temperatures and high voltages [29–31].

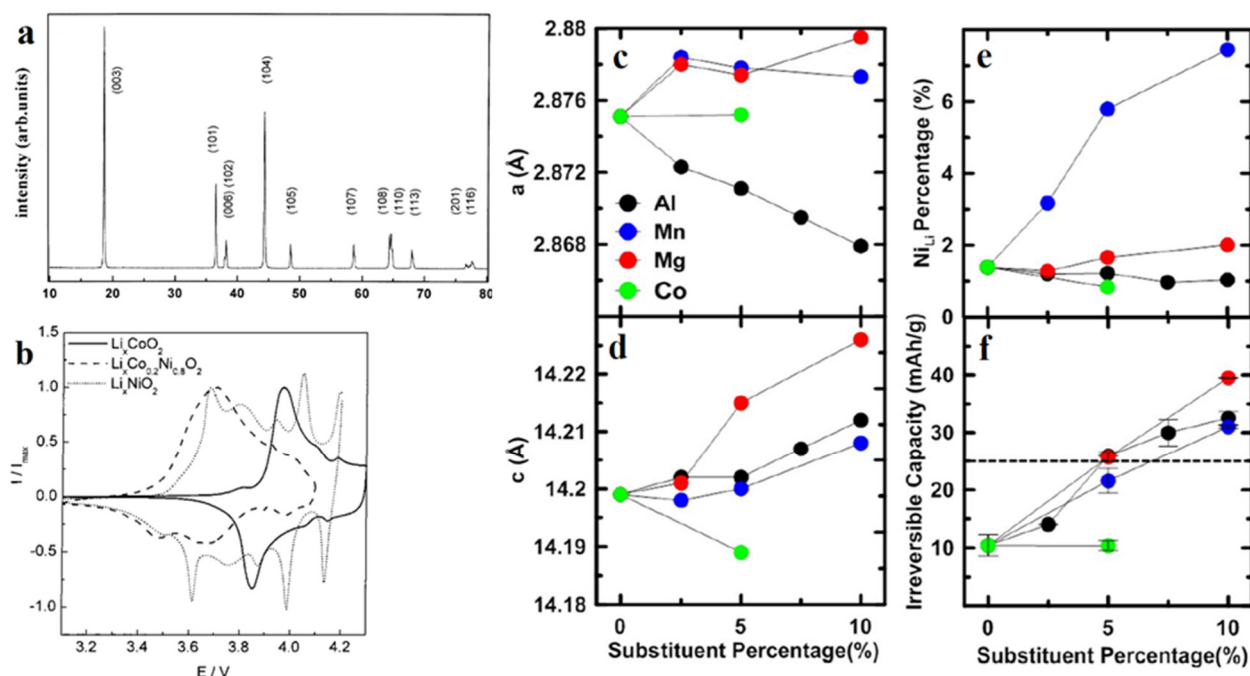


Figure 2. (a) XRD of LNO, reproduced with permission [32], (b) cyclic voltammetry of LCO-, LNO, and Co-doped LNO, reproduced with permission [24], (c) substituent percentage vs. a-axis, (d) substituent percentage vs. c axis, (e) substituent percentage vs. NiLi, and (f) substituent percentage vs. irreversible capacity [8].

As seen in the composition of the NMC, cobalt, which substitutes nickel, has an effective role in stabilizing Ni^{2+} ions in the structure of the layered-transition metal, thereby reducing the level of mixing between Li^+ / Ni^{2+} cations [33]. However, there is one recent study that questioned whether the role of cobalt is really irreplaceable by other metals to have the same effect [8]. Recent research conducted by Li et al. has confused the previous theory regarding the effect of cobalt in nickel-rich layered-transition metal cathodes by systematically studying various compositions of cobalt replacement cations in the $\text{LiNi}_{1-x}\text{M}_x\text{O}_2$ composition ($\text{M} = \text{Al, Co, Mg, or Mn}; x = 0.05 \text{ or } 0.1$). As previously stated, the role of Co is to reduce the mixing level of Li^+ / Ni^{2+} cations, but the XRD results of this study (Figure 2c,d) show that for Mn-free materials, Co does not significantly contribute to the reduction of the mixing of Li^+ / Ni^{2+} cations. This is evidenced in the increase in the percentage of Ni atoms as the percentage of Mn atoms increases (Figure 2e), which is expected because more Mn^{4+} will be compensated by more Ni^{2+} ions. The Al and Mg series without Co shows low mixing of Li^+ / Ni^{2+} cation. Figure 2f shows that as the dopant content rises, the irreversible capacity rises with it.

Furthermore, this study reported that $\text{LiNi}_{0.95}\text{Mg}_{0.05}\text{O}_2$ yielded a lower initial discharge capacity of 205 mAh g^{-1} at a current density of 10 mA g^{-1} , when compared to $\text{LiNi}_{0.95}\text{Mn}_{0.05}\text{O}_2$ of 219 mAh g^{-1} and $\text{LiNi}_{0.95}\text{Al}_{0.05}\text{O}_2$ of 223 mAh g^{-1} as shown in Figure 3a. This is attributed to the presence of Mg, which causes the position of the Li atom to share space with the upper and lower layers, i.e., two Li atoms become inactive due to the presence of one Mg atom, weakening the attraction between the layers, which causes phase changes. This certainly affects the reversible capacity of the cathode. This research also reported no real increase in the structural stability during the cycle of $\text{LiNi}_{0.95}\text{Co}_{0.05}\text{O}_2$ when compared to all tested samples. The initial discharge capacity and cycle stability of $\text{LiNi}_{0.95}\text{Al}_{0.05}\text{O}_2$ are similar to that of NCA, with capacity retention of 95% of the initial capacity after 50 cycles and a current density of 10 mA g^{-1} . Meanwhile, $\text{LiNi}_{0.95}\text{Mg}_{0.05}\text{O}_2$ has better capacity retention of 97% after 50 cycles but with a lower initial specific discharge. This suggests that cobalt does not contribute to capacity retention in the long term.

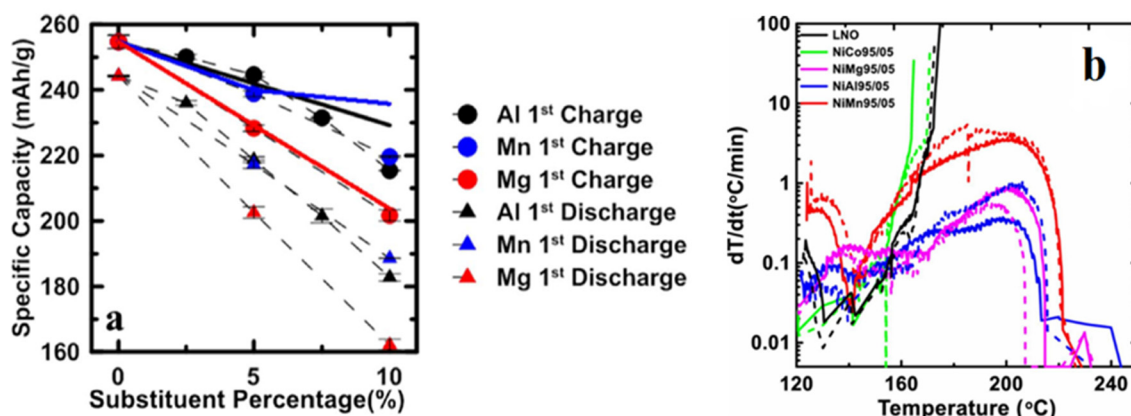


Figure 3. (a) Initial discharge capacity as a function of Al, Mn, and Mg percentage; and (b) self-heating rate of the delithiated LiNiO_2 and $\text{LiNi}_{0.95}\text{M}_{0.05}\text{O}_2$ ($\text{M} = \text{Co}, \text{Mg}, \text{Al}$ or Mn) [8].

In addition, this study shows that cobalt substitution ($\text{LiNi}_{0.95}\text{Co}_{0.05}\text{O}_2$) does not improve the thermal stability compared to $\text{LiNi}_{0.95}\text{Mg}_{0.05}\text{O}_2$, $\text{LiNi}_{0.95}\text{Al}_{0.05}\text{O}_2$, and $\text{LiNi}_{0.95}\text{Mn}_{0.05}\text{O}_2$ with a self-heating rate $>20\text{ }^\circ\text{C min}^{-1}$ at $160\text{ }^\circ\text{C}$. On the other hand, Al and Mg show a significant contribution with self-heating rate $<1\text{ }^\circ\text{C min}^{-1}$ for the range of $120\text{--}240\text{ }^\circ\text{C}$ (Figure 3b). Here, it can be seen that the contribution of Co is not significant in reducing the self-heating rate of the LNO-based cathode. Even in some other results, the addition of Co shows an increase in the internal heat when fully charged [34–36]. Therefore, this research report questions the role of cobalt in the Ni-rich layered-transition metal oxide material by comparing its electrochemical performance with other metal dopants.

The discussion of promising high-Ni NMC-layered material has been outlined, mainly reducing the cost, increasing the capacity, and reducing the risk on the supply of cobalt. However, the cathode lifetime is limited because of its structural degradation on the subsurface of high-Ni NMC. The degradations change the interfaces and properties. It is widely known that higher cut-off potential and elevated temperature are responsible for the degradation of the high-Ni NMC [37–40]. It has been reported that in situ XRD experiments with a slow enough rate of C/50, the lattice parameter of $\text{LiNi}_{0.8}\text{Mn}_{0.1}\text{Co}_{0.1}\text{O}_2$ (NMC811) appears to have a non-monotonic dependence on the Li content, and the lattice changes thus become highly anisotropic [41]. A comparative study conducted by Kondakov et al. [38] indicates that the volume changes in NMC811 are more significant than those of $\text{LiNi}_{1/3}\text{Mn}_{1/3}\text{Co}_{1/3}\text{O}_2$ (NMC111) at a potential between 4.0 and 4.3 V. The temperature of the battery comprised with high-Ni NMC should be closely monitored because it is directly related to the safety of the battery operation. At a high SOC, the spontaneous reduction of Ni^{4+} to Ni^{2+} during heating accompanied by the release of oxygen causes the destruction of the original structure [18,42,43]. Nevertheless, the current research shows that intrinsic degradation leads to subsurface structural changes and some deposited products presented in Figure 4a. The structural degradation of the layered structure becoming a rock-salt structure on the surface leads to a limited diffusion for Li^+ . Other degradation mechanisms include metals dissolution, oxygen release, and surface reaction with electrolyte, leading to a release of CO/CO_2 [44]. In many cases, the dissolution of the transition metals (TMs) from the bulk diffuses into the anode and thickens the SEI on the anode, as shown in Figure 4b. In addition to the degradation that originated from the cathode, the degradation can also occur from the trace of water. Water traces react with the electrolyte, LiPF_6 , and form HF. This leads to the acid attack of TMs by the HF [45].

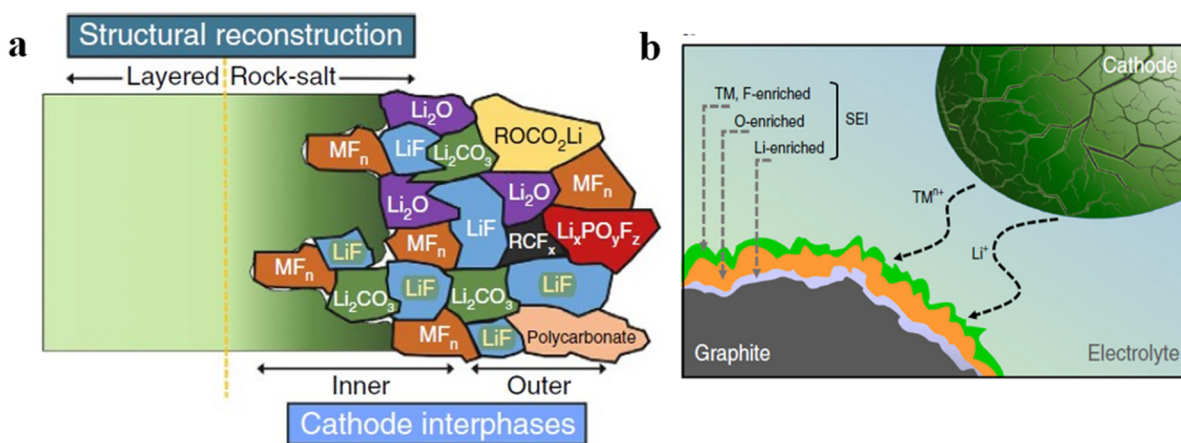


Figure 4. (a) Structure of the Ni-rich NMC electrode-electrolyte interface formed after several cycles showing several Li-based compounds and TM-based compounds [46] and (b) the dissolved TMs enriched the SEI on the anode surface [47].

3. Strategy to Reduce Cobalt in LIBs

3.1. Doping with Other Transition Metals

Various types of cations have been studied as alternatives to cobalt in Ni-rich cathodes over the past few years using Mg^{2+} , Al^{3+} , Fe^{3+} , and Na^+ cations, which have shown significant progress in electrochemical performance and safety factors [48–50]. In addition, significant results have been achieved to understand the relationship between the cathode dopants, thermal stability, and reactivity with electrolytes. In the case of thermal stability, under ambient conditions, Ni-rich cathodes in their charged states are metastable. Because of the highly effective oxygen partial pressure, they begin to break down and emit O_2 at high temperatures ($>200^\circ\text{C}$). The emitted O_2 can then react with the organic solvent, resulting in a thermal runaway.

It was reported that the thermal stability could be improved in $\text{LiNi}_x\text{M}_{1-x}\text{O}_2$ by substituting the dopant Mn, Mg, Al, or Co in which $x = 0$ or 0.05 (Figure 5) [51]. Al- and Mg-doped LNO shows the highest stability to the thermal decomposition among other samples. The decomposition is expected to have two steps; namely, the first step corresponds to the phase transformation from a layered-material to a spinel structure followed by oxygen evolution around 200°C , and the second step is related to the formation of the rock-salt phase with more evolution of oxygen from the structure at elevated temperature [52,53]. Interestingly, Al-doped LNO shows that the second step is delayed due to a stronger bond of Al^{3+} with oxygen. This could suppress the cation migration for the phase transformation with increasing temperature [54]. In addition, the dopant effect can also increase the Li content at a higher charge voltage of 4.4 V versus Li^+/Li , which reduces the evolution of oxygen and makes the structure more stable. The effect of dopants also shows that the reduction of side reactions with electrolytes causes a much higher thermal stability (220°C) compared to that without dopants in $\text{LiNi}_{0.95}\text{Co}_{0.05}\text{O}_2$.

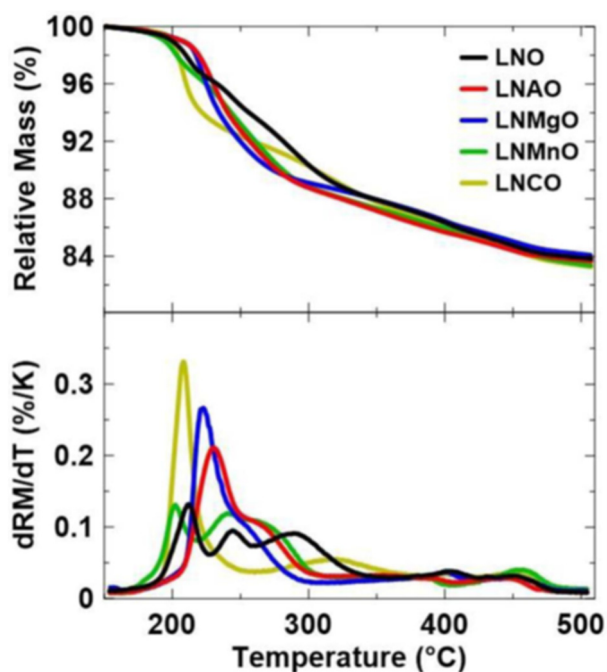


Figure 5. Thermal stability of $\text{LiNi}_x\text{M}_{1-x}\text{O}_2$ by substituting the dopant Mn, Mg, Al, or Co in which $x = 0$ or 0.05 [51].

Another study reported the effect of Mn dopant on the electrochemical performance of $\text{LiNi}_{0.9}\text{Mn}_{0.1}\text{O}_2$, which is the development of the most studied cobalt-free nickel-rich cathode material, $\text{LiNi}_{0.5}\text{Mn}_{0.5}\text{O}_2$ [55]. $\text{LiNi}_{0.9}\text{Mn}_{0.1}\text{O}_2$ shows an increase in the capacity stability with an initial discharge capacity of 227 mAh g^{-1} at 0.1 C as a function of Mn, which can maintain its discharge capacity up to 93% after 100 cycles. This is related to the role of the inactive Mn^{4+} ion, which can stabilize the structure during the delithiation process, as evidenced by the change in the redox potential associated with the $\text{H}_2 \rightarrow \text{H}_3$ phase transition. The broadening of the dQ/dV peaks indicates that there has been a change in the volumetric lattice, which allows the inhomogeneous strain relaxation in the crystal lattice. In addition, the fracture strength of the $\text{LiNi}_{0.9}\text{Mn}_{0.1}\text{O}_2$ particles was 25% higher than that to $\text{LiNi}_{0.9}\text{Mn}_{0.05}\text{Co}_{0.05}\text{O}_2$ (140 MPa). These two mechanisms demonstrate the important role of Mn in improving the cycle stability in LiNiO_2 -based materials. Although the addition of Mn improves the electrochemical stability, Mn dissolution is a serious problem in Mn-based cathode materials for LIBs, mainly at high voltages. It is reported that $\text{Li}_2\text{Mn}_{1-x}\text{Ti}_x\text{O}_2\text{F}$ ($0 \leq x \leq 2/3$) material [56], despite the absence of severe delithiation, demonstrates a significant loss of capacity after continuous cycling at high voltage due to the dissolution of Mn ions into the electrolyte. The electrochemical performance of $\text{LiNi}_{0.8}\text{Mg}_{0.2}\text{O}_2$ was also investigated and obtained specific discharge capacity of 185 mAh g^{-1} at 0.1 mA cm^{-2} but was only stable for 25 cycles [57]. The specific discharge capacity of $\text{LiNi}_{0.8}\text{Al}_{0.2}\text{O}_2$ is observed at about 150 mAh g^{-1} at 0.17 mA cm^{-2} and generates the formation of an insulating material when fully charged [58]. Among Mn-, Mg-, Al-, or Co-doped LNO materials, $\text{Li}[\text{Ni}_{0.9}\text{Co}_{0.1}]\text{O}_2$ delivers the highest specific discharge capacity of 233 mAh g^{-1} at 0.1 C . However, it experiences severe capacity fading of 77% [59]. This is attributed to a developed microcrack on an entire particle when it is charged to 4.3 V , exposing the internal particle to electrolyte attack.

3.2. Particles and Synthesis Engineering

A large number of studies [51,55,60] has been carried out over the past few years in an effort to improve the electrochemical performance of the cathode material of high-nickel composition $\text{LiNi}_{1-x}\text{M}_x\text{O}_2$ ($M = \text{Mn, Al, and/or Co}$) so that dependence on cobalt can be reduced. Nickel-rich cathodes, such as NMC811 and NCA, are one step forward to

developing LiNiO_2 (LNO)-based cathode materials that are completely cobalt-free. This is because the LNO has a high energy density in line with the target of LIB performance for EVs in the future. However, thermal instability [54,61] and structural decomposition significantly decrease the electrochemical performance of LNO-based materials [33,62]. This is the main barrier for the commercial application of this type of cathode material for modern LIB applications. Mixing Li^+ / Ni^{2+} cation during the charge-discharge process is one of the main obstacles of Ni-rich cathode, inducing the local formation of inactive rock-salt phases that can worsen the battery performance during the charge-discharge process.

One strategy for overcoming this challenge is to synthesize NMC at the micron scale of single crystal particles [63–66]. Compared with the polycrystalline NMC, which consists of agglomerated particles measuring 10 to 15 μm , the single crystal morphology has the fewest grain boundaries, thereby reducing particle cracking and side effects with electrolytes (Figure 6a,b) [67]. A single crystal does not have grain boundaries inside one particle, thus providing a continuous Li^+ pathway. In contrast, Li^+ needs to pass through many grain boundaries in the polycrystalline, as seen in Figure 6c,d. It was also reported that the single-crystal $\text{Li}(\text{Ni}_{0.5}\text{Mn}_{0.3}\text{Co}_{0.2})\text{O}_2$ applied as a cathode material for all-solid-state lithium-ion batteries exhibits 6–14 times higher Li^+ diffusion coefficient than polycrystalline $\text{Li}(\text{Ni}_{0.5}\text{Mn}_{0.3}\text{Co}_{0.2})\text{O}_2$ [68]. The single crystal $\text{LiNi}_{0.5}\text{Co}_{0.2}\text{Mn}_{0.3}\text{O}_2$ with uniform size distribution and a polyhedron single-crystal structure using glucose and urea in one pot is successfully synthesized by a hydrothermal process which shows a promising initial electrochemical performance [69]. The single-crystal NMC523 shows a highly ordered hexagonal arrangement in a-b plane and a minimized antisite mixing of $\text{Ni}^{2+}/\text{Li}^+$.

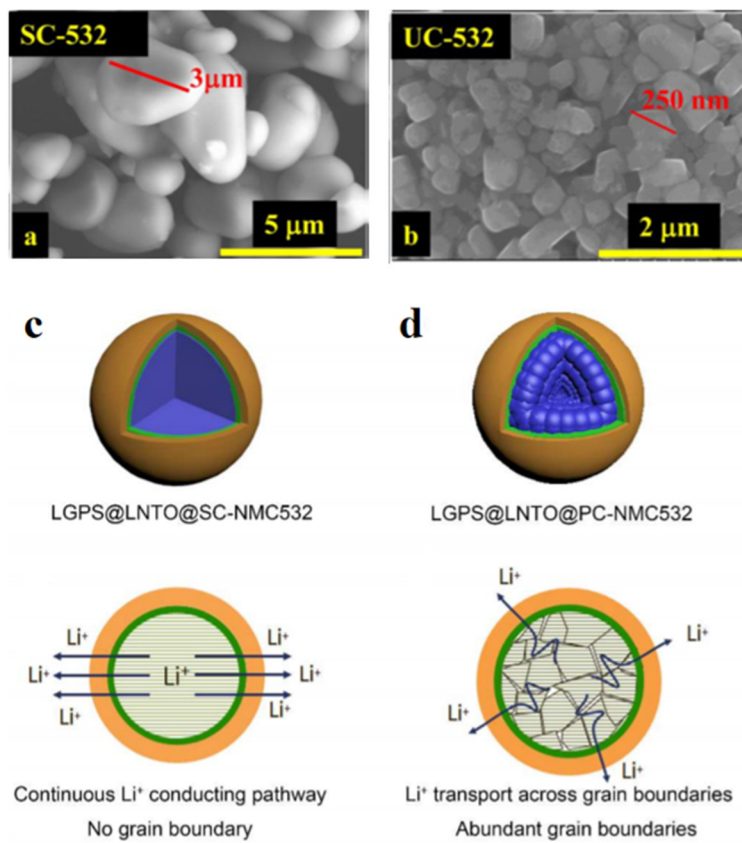


Figure 6. SEM images of single-crystalline and polycrystalline structure of NMC (a,b) [67], and illustration of the Li^+ transport in single and polycrystalline (c,d) [68].

The next strategy is to design and engineer nanoparticle structures for cobalt-free cathodes that have been carried out in several research activities in recent years [70–75].

The core-shell structure for Ni-rich NMC materials, in which the core contains more Ni while the shell is richer in Mn, was previously investigated. This strategy can reduce volume expansion and protect the core from electrolyte reactions [76–78]. It is reported that the LiNiO₂ core with the LiNi_{0.83}Mg_{0.17}O₂ shell is capable of providing an initial discharge capacity of 194 mAh g⁻¹ and 230 mAh g⁻¹ for the LiNi_{0.83}Al_{0.17}O₂ shell and Li-Ni_{0.83}Mn_{0.17}O₂ shell at 0.2 C. In addition, cathodes with the LNO-LiNi_{0.83}Mg_{0.17}O₂ and LNO-Li-Ni_{0.83}Mn_{0.17}O₂ core-shell structures were able to maintain 94 and 92% of their initial capacity, respectively, after 55 cycles, while the LNO-LiNi_{0.83}Al_{0.17}O₂ electrodes maintained 93% of the initial capacity after 55 cycles at 0.2 C. Although the capacity obtained is quite high, the metal dopant diffuses from the shell to the core structure during the sintering process, indicating that the core-shell structure was not fully successful. However, the report shows promising results and offers a chance for process improvement by utilizing a more optimal synthesis pathway.

It was also reported that Wang et al. succeeded in synthesizing Li-rich Li_{1.2}Mn_{0.6}Ni_{0.2}O₂ with a morphology of a porous nanoflake-shaped structure through the sol-gel method with the aid of resorcinol-formaldehyde [79]. The porous nanoflake structure has a specific surface area of 6.9 m² g⁻¹, which is higher than that of the spherical structure which has a surface area of only 1.5 m² g⁻¹ [80]. The high surface area facilitates the diffusion of lithium, resulting in increased rate performance, with discharge capacities of 273 mAh g⁻¹ at 0.1 C and 196 mAh g⁻¹ at 2 C from 2.0–4.8 V versus Li⁺/Li. This structure form usually causes a decrease in electrochemical stability because the high surface area promotes an increase in the SEI formation process and a high Li consumption rate. However, the reported results showed that the capacity obtained was relatively stable with a retention of 93% after 150 cycles at 2 C, which indicated that the material stability was not significantly affected due to morphological modification.

Further development for the cycle enhancement of cobalt-free cathode materials is done by synthesizing the Li-rich layered oxide material with type O₂ oxides which can suppress H₂ → H₃ phase transitions [81]. The synthesis method used is unique to prepare this material, namely by the ionic exchange process of Na⁺ with Li⁺ in the form of the compound P2 Na_{0.83} [Li_{0.19}Mn_{0.73}Ni_{0.08}]O₂ in a liquid salt solution, resulting in material rich in Li₂O₂-Li_{1.19-y}Mn_{0.73}Ni_{0.08}O₂. This material achieved an initial discharge capacity of 240 mAh g⁻¹ at 0.05 C. The material also showed excellent capacity retention compared to O₃-type materials, which was able to maintain more than 90% of the initial capacity after 50 cycles. These results suggest that the modification of the crystal structure through this synthesis procedure can be one of the keys to developing the next generation of cobalt-free cathode materials.

Modifications to the particle surface and coating techniques have also been investigated as solutions to improve the stability and performance of cobalt-free cathodes [82–89]. In general, the coating functions as a barrier and protection between the electrolytes and active ingredients, reducing the influence of acidity from electrolytes and substantially limiting the dissolving metal ions from the cathode during the cycle process [90–92]. It was reported that thioacetamide (TA)-supported ZrO₂ coating on the surface of the Ni-rich layered oxide LiNi_{0.82}Mn_{0.09}Co_{0.09}O₂ (NMC82) has an enhanced rate capability of 116.8 mAh g⁻¹ at 3.0 C [93]. The dual Al-Zr incorporated Ni-rich cathode was a self-formed interfacial protective layer that effectively reduces the formation of cation mixing and the generation of microcracks [94]. One of the most significant results of a recent study was presented by Deng et al., who designed the SEI layer to be rich in the F-B element in LiNiO₂ by adding a small amount of difluoro (oxalato) borate (LiDFOB) in the electrolyte, as shown in Figure 7 [95]. The obtained result is a strong and compact SEI layer that is able to reduce the release of Ni and prevent unwanted phase transformations, namely the NiO rock-salt phase by protecting the surface of the active material from reacting with by-products resulting from electrolyte oxidation at high voltage. This material shows a high initial discharge capacity of 216 mAh g⁻¹ with capacity stability of 94% after 100 cycles.

In comparison, LNO without the additive LiDFOB was only able to maintain 18% of the initial capacity after 100 cycles.

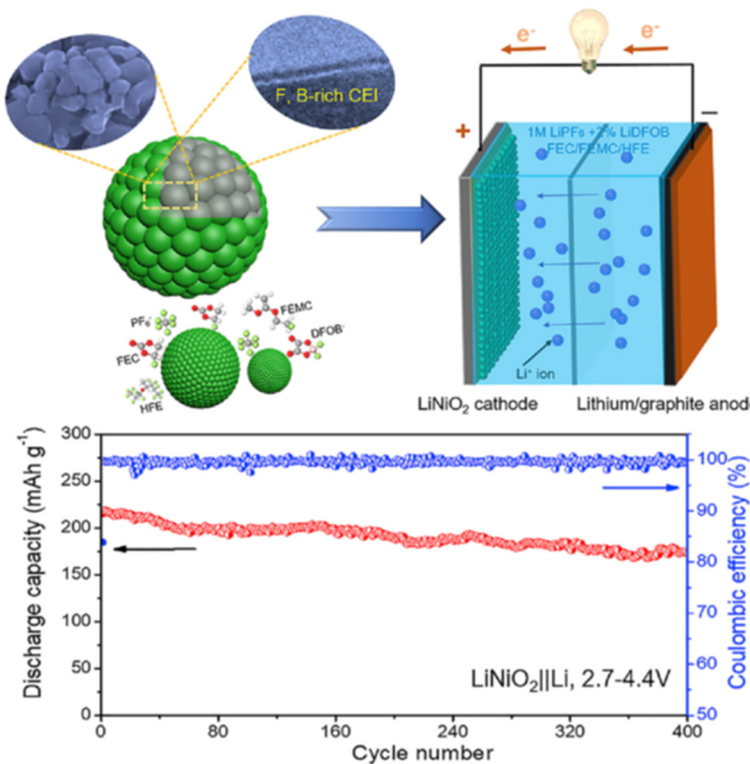


Figure 7. In situ formation of F and B-rich SEI layer on cobalt-free LiNiO₂ and long-term cycling ability and Coulombic efficiency over 400 cycles at 0.5 C. [95].

A recent investigation has reported a new type of material for cobalt-free high-nickel cathodes, namely $\text{LiNi}_{1-x-y}\text{Mn}_x\text{Al}_y\text{O}_2$ (NMA), which has been synthesized successfully with overall superior electrochemical performance compared to NMC and NCA for lithium batteries [96]. In this report, $\text{LiNi}_{0.883}\text{Mn}_{0.056}\text{Al}_{0.061}\text{O}_2$ (NMA-89) has a comparable specific discharge capacity of 216 mAh g^{-1} with $\text{LiNi}_{0.890}\text{Mn}_{0.055}\text{Co}_{0.055}\text{O}_2$ (NMC-89) and $\text{LiNi}_{0.883}\text{Co}_{0.053}\text{Al}_{0.064}\text{O}_2$ (NCA-89) (226 mAh g^{-1} and 220 mAh g^{-1}) as shown in Figure 8a. NMA-89 also shows a higher operating voltage, about 40 mV, than NMC-89 (Figure 8b). Figure 8c shows that the rate capability of NMA-89 is very similar to that of NMC-89 and NCA-89. The capacity retention of NMA-89 after 100 cycles at a C/3 rate (90%) is comparable to NMC-89 (91%) and even with NCA-89 (88%) as seen in inset Figure 8a.

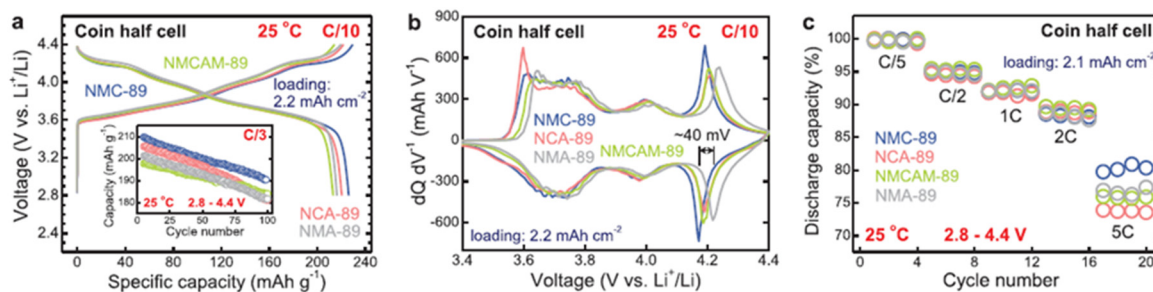


Figure 8. Electrochemical performance of NMA89 compared with NMC89, NCA89 and NCMAM89. (a) Galvanostatic charge-discharge profile curves at 0.1 C, (b) dQ/dN curves, and (c) rate capability performance. Image is adapted with permission from authors [96]. Reproduced from Advanced Materials, the name of the publisher: John Wiley and Sons.

NMA with various compositions, namely, $\text{LiNi}_{0.80}\text{Mn}_{0.13}\text{Al}_{0.07}\text{O}_2$, $\text{LiNi}_{0.85}\text{Mn}_{0.09}\text{Al}_{0.06}\text{O}_2$, $\text{LiNi}_{0.88}\text{Mn}_{0.07}\text{Al}_{0.05}\text{O}_2$, $\text{LiNi}_{0.90}\text{Mn}_{0.06}\text{Al}_{0.04}\text{O}_2$, and $\text{LiNi}_{0.92}\text{Mn}_{0.05}\text{Al}_{0.03}\text{O}_2$ can be engineered to meet various electrochemical performance targets. In terms of the scalability of the synthesis, the coprecipitation of Al is more complex than Ni, Co, and Mn. Stabilization techniques using the doping method approach and surface passivation of particles were also carried out in NMAs. However, there is still much that needs to be studied regarding the electrochemical characterization, such as understanding the benefits and disadvantages of Mn-Al substitution in Ni-rich layered oxides in the absence of Co, in industrial-scale cell configurations, and in various operating conditions. Furthermore, the moisture sensitivity of NMA with high Ni content should also be anticipated as in NMC and NCA, and of course, more analysis of the phenomena during the cycle must be considered.

Table 1 shows a summary of Ni-rich Co-less cathode materials that have been developed and synthesized by many researchers through coating and surface modification, nanostructured morphology, and effective doping. Generally, all Ni-rich Co-less cathode materials exhibit cycling stability and high energy density. The interphase stability between the electrode and electrolyte is enhanced through the surface and structural modification. Gradually decreasing the Ni concentration from the inner core to the outer layer is beneficial for improving capacity fading.

Table 1. Summary of the Ni-rich Co-less cathode materials and their electrochemical performance.

Materials System	Modification/Treatment	Voltage (V)	Capacity (mAh g ⁻¹)	Capacity Retention	Heat Generation (J g ⁻¹)	Refs.
$\text{Li}[\text{Ni}_{0.885}\text{Co}_{0.100}\text{Al}_{0.015}\text{O}_2]$	Multi-doped (Ga, B) Ni-rich core and Co-rich particle surface	2.7–4.3	222.2	91.7% at 0.5 C after 100 cycles	-	[97]
$\text{Li}[\text{Ni}_{0.865}\text{Co}_{0.120}\text{Al}_{0.015}\text{O}_2]$	-	2.7–4.3	222	90.0% at 0.5 C after 100 cycles	1409	[98]
$\text{Li}[\text{Ni}_{0.89}\text{Co}_{0.05}\text{Mn}_{0.05}\text{Al}_{0.01}\text{O}_2]$	-	2.7–4.3	228	87.1% at 0.5 C after 100 cycles	1384	[99]
$\text{Li}[\text{Ni}_{0.85}\text{Co}_{0.05}\text{Mn}_{0.10}\text{O}_2]$	-	2.7–4.3	222	93.5% at 0.5 C after 100 cycles	-	[100]
$\text{Li}[\text{Ni}_{0.84}\text{Co}_{0.06}\text{Mn}_{0.09}\text{Al}_{0.01}\text{O}_2]$	Two-step concentration gradients	2.7–4.3	221	96.4% at 0.5 C after 100 cycles	-	[101]
$\text{Li}[(\text{Ni}_{0.8}\text{Co}_{0.1}\text{Mn}_{0.1})_0.8(\text{Ni}_{0.5}\text{Mn}_{0.5})_0.2\text{O}_2]$	Spherical core–shell structure	3.0–4.3	180	100% at 0.5 C after 100 cycles	-	[102]
$\text{Li}[\text{Ni}_{0.886}\text{Co}_{0.049}\text{Mn}_{0.050}\text{Al}_{0.015}\text{O}_2]$	Hybrid cathode with core–shell structure	2.7–4.3	215	96.1% at 0.5 C after 100 cycles	-	[103]
$\text{Li}[\text{Ni}_{0.90}\text{Co}_{0.05}\text{Mn}_{0.05}\text{O}_2]$	Hybrid cathode	2.7–4.3	225	87.7% at 0.5 C after 100 cycles	1561	[99]
$\text{Li}[\text{Ni}_{0.9}\text{Co}_{0.05}\text{Mn}_{0.05}\text{O}_2]$	Hybrid cathode	2.7–4.3	228.7	92.2% at 0.5 C after 100 cycles	-	[104]
LiNiO_2	-	2.7–4.3	247.5	73.7% at 0.5 C after 100 cycles	1827	[105]
$\text{LiNi}_{0.99}\text{W}_{0.01}\text{O}_2$	Tungsten-doped	2.7–4.3	242.7	90.3% at 0.5 C after 100 cycles	1309	[106]
$\text{LiNi}_{0.985}\text{W}_{0.015}\text{O}_2$	Tungsten-doped	2.7–4.3	236.1	93.5% at 0.5 C after 100 cycles	1235	[106]
$\text{LiNi}_{0.9}\text{Mn}_{0.1}\text{O}_2$	-	2.7–4.3	212.3	93% at 0.5 C after 150 cycles	794.6	[107]

4. Conclusions and Perspectives

Until now, LiCoO_2 has been the main option for LIBs since the introduction by Goodenough et al. in 1980, followed by the commercialization of LIBs by SONY. Although LiCoO_2 offers benefits in terms of high theoretical specific capacity, high discharge voltage, low self-discharge, and superior cyclability, the high processing cost of raw cobalt and severe capacity fading at high current loads remain a challenge. With the expansion of the automotive industry focusing on the development of EVs, the concern to reduce the cobalt utilization in the cathode is taken into consideration by researchers. The demand for high-density energy from LIBs has led to several studies on Ni-rich layered-transition metal oxides of LiNiO_2 -based materials. Various strategies have been reported to enhance the electrochemical properties of Ni-rich LiNiO_2 -based cathodes as an alternative to LiCoO_2 , including cation doping, structural design, surface modification, and coating. Potential problems that arise in cobalt-free Ni-rich cathodes based on LiNiO_2 are related to cycle stability, which is closely related to the volume expansion factor, the fragility of particles due to high Li^+ content, mixing of $\text{Ni}^{2+}/\text{Li}^+$ cations, increased electrolyte oxidation, and thermal stability. By preventing phase transformation and particle breakdown, partial substitution of Co atoms with Mn, Al, and Mg atoms improves thermal stability and cycle stability. In fact, Mn doping on LiNiO_2 does not affect the initial discharge capacity but results in an increased degree of mixing of $\text{Ni}^{2+}/\text{Li}^+$ cations. Conversely, Al and Mg doping can help suppress the mixing of $\text{Ni}^{2+}/\text{Li}^+$ cations but at the sacrifice of the initial discharge capacity. For this reason, the best strategy to achieve optimal performance is to combine the cation doping method with morphological control and a coating method that increases the

conductivity between particles while providing a barrier against electrolyte side reactions in the form of a protective layer and controlling the oxide crystal structure to reduce phase transformation. Research in this direction is expected to be able to provide solutions for the short term so that the commercialization of cobalt-free high-Ni cathodes will soon be realized.

Author Contributions: Conceptualization, L.N. and S.S.; data curation, L.N.; writing—original draft preparation, L.N. and S.S.; writing—review and editing, L.N., S.S., N.H.I. and H.K.D.; project administration, S.S.; funding acquisition, S.S. All authors have read and agreed to the published version of the manuscript.

Funding: This research was partially funded by the Indonesian Ministry of Research and Technology/National Agency for Research and Innovation and the Indonesian Ministry of Education and Culture, under the World Class University Program managed by Institut Teknologi Bandung.

Institutional Review Board Statement: Not applicable.

Informed Consent Statement: Not applicable.

Data Availability Statement: Not applicable.

Conflicts of Interest: The authors declare no conflict of interest.

References

1. Gourley, S.W.D.; Or, T.; Chen, Z. Breaking Free from Cobalt Reliance in Lithium-Ion Batteries. *iScience* **2020**, *23*, 101505. [[CrossRef](#)]
2. Cano, Z.P.; Banham, D.; Ye, S.; Hintennach, A.; Lu, J.; Fowler, M.; Chen, Z. Batteries and fuel cells for emerging electric vehicle markets. *Nat. Energy* **2018**, *3*, 279–289. [[CrossRef](#)]
3. Dahn, J.R.; von Sacken, U.; Michal, C.A. Structure and electrochemistry of $\text{Li}_{1\pm y}\text{NiO}_2$ and a new Li_2NiO_2 phase with the $\text{Ni}(\text{OH})_2$ structure. *Solid State Ion.* **1990**, *44*, 87–97. [[CrossRef](#)]
4. Whittingham, M.S. Lithium Batteries and Cathode Materials. *Chem. Rev.* **2004**, *104*, 4271–4302. [[CrossRef](#)]
5. Thomas, M.G.S.R.; David, W.I.F.; Goodenough, J.B.; Groves, P. Synthesis and structural characterization of the normal spinel $\text{Li}[\text{Ni}_2]\text{O}_4$. *Mater. Res. Bull.* **1985**, *20*, 1137–1146. [[CrossRef](#)]
6. Liu, W.; Oh, P.; Liu, X.; Lee, M.-J.; Cho, W.; Chae, S.; Kim, Y.; Cho, J. Nickel-Rich Layered Lithium Transition-Metal Oxide for High-Energy Lithium-Ion Batteries. *Angew. Chem. Int. Ed.* **2015**, *54*, 4440–4457. [[CrossRef](#)]
7. Ohzuku, T.; Ueda, A.; Nagayama, M.; Iwakoshi, Y.; Komori, H. Comparative study of LiCoO_2 , $\text{LiNi}_{12}\text{Co}_{12}\text{O}_2$ and LiNiO_2 for 4 volt secondary lithium cells. *Electrochim. Acta* **1993**, *38*, 1159–1167. [[CrossRef](#)]
8. Li, H.; Cormier, M.; Zhang, N.; Inglis, J.; Li, J.; Dahn, J.R. Is Cobalt Needed in Ni-Rich Positive Electrode Materials for Lithium Ion Batteries? *J. Electrochem. Soc.* **2019**, *166*, A429–A439. [[CrossRef](#)]
9. Mu, L.; Zhang, R.; Kan, W.H.; Zhang, Y.; Li, L.; Kuai, C.; Zytlewski, B.; Rahman, M.M.; Sun, C.-J.; Sainio, S.; et al. Dopant Distribution in Co-Free High-Energy Layered Cathode Materials. *Chem. Mater.* **2019**, *31*, 9769–9776. [[CrossRef](#)]
10. Kim, Y.; Seong, W.M.; Manthiram, A. Cobalt-free, high-nickel layered oxide cathodes for lithium-ion batteries: Progress, challenges, and perspectives. *Energy Storage Mater.* **2021**, *34*, 250–259. [[CrossRef](#)]
11. Li, W.; Erickson, E.M.; Manthiram, A. High-nickel layered oxide cathodes for lithium-based automotive batteries. *Nat. Energy* **2020**, *5*, 26–34. [[CrossRef](#)]
12. Berckmans, G.; Messagie, M.; Smekens, J.; Omar, N.; Vanhaverbeke, L.; Mierlo, J. Van Cost Projection of State of the Art Lithium-Ion Batteries for Electric Vehicles Up to 2030. *Energies* **2017**, *10*, 1314. [[CrossRef](#)]
13. Few, S.; Schmidt, O.; Offer, G.J.; Brandon, N.; Nelson, J.; Gambhir, A. Prospective improvements in cost and cycle life of off-grid lithium-ion battery packs: An analysis informed by expert elicitation. *Energy Policy* **2018**, *114*, 578–590. [[CrossRef](#)]
14. Ballinger, B.; Stringer, M.; Schmeda-Lopez, D.R.; Kefford, B.; Parkinson, B.; Greig, C.; Smart, S. The vulnerability of electric vehicle deployment to critical mineral supply. *Appl. Energy* **2019**, *255*, 113844. [[CrossRef](#)]
15. Gulley, A.L.; McCullough, E.A.; Shedd, K.B. China's domestic and foreign influence in the global cobalt supply chain. *Resour. Policy* **2019**, *62*, 317–323. [[CrossRef](#)]
16. Zeng, X.; Li, M.; Abd El-Hady, D.; Alshitari, W.; Al-Bogami, A.S.; Lu, J.; Amine, K. Commercialization of Lithium Battery Technologies for Electric Vehicles. *Adv. Energy Mater.* **2019**, *9*, 1900161. [[CrossRef](#)]
17. Overland, I. The geopolitics of renewable energy: Debunking four emerging myths. *Energy Res. Soc. Sci.* **2019**, *49*, 36–40. [[CrossRef](#)]
18. Noh, H.-J.; Youn, S.; Yoon, C.S.; Sun, Y.-K. Comparison of the structural and electrochemical properties of layered $\text{Li}[\text{Ni}_x\text{Co}_y\text{Mn}_z]\text{O}_2$ ($x = 1/3$, 0.5, 0.6, 0.7, 0.8 and 0.85) cathode material for lithium-ion batteries. *J. Power Sources* **2013**, *233*, 121–130. [[CrossRef](#)]
19. Saadoune, I.; Delmas, C. On the $\text{Li}_x\text{Ni}_{0.8}\text{Co}_{0.2}\text{O}_2$ System. *J. Solid State Chem.* **1998**, *136*, 8–15. [[CrossRef](#)]

20. Zhecheva, E.; Stoyanova, R. Stabilization of the layered crystal structure of LiNiO_2 by Co-substitution. *Solid State Ion.* **1993**, *66*, 143–149. [[CrossRef](#)]
21. Zeng, X.; Zhan, C.; Lu, J.; Amine, K. Stabilization of a High-Capacity and High-Power Nickel-Based Cathode for Li-Ion Batteries. *Chem.* **2018**, *4*, 690–704. [[CrossRef](#)]
22. Wan, H.; Liu, Z.; Liu, G.; Yi, S.; Yan, P.; Deng, H.; Hu, W.; Gao, F. Unraveling TM Migration Mechanisms in $\text{LiNi}_{1/3}\text{Mn}_{1/3}\text{Co}_{1/3}\text{O}_2$ by Modeling and Experimental Studies. *Nano Lett.* **2021**, *21*, 6875–6881. [[CrossRef](#)]
23. Moses, A.W.; Flores, H.G.G.; Kim, J.-G.; Langell, M.A. Surface properties of LiCoO_2 , LiNiO_2 and $\text{LiNi}_{1-x}\text{CoxO}_2$. *Appl. Surf. Sci.* **2007**, *253*, 4782–4791. [[CrossRef](#)]
24. Nobili, F.; Croce, F.; Scrosati, B.; Marassi, R. Electronic and Electrochemical Properties of $\text{Li}_x\text{Ni}_{1-y}\text{CoyO}_{1/3}$ Cathodes Studied by Impedance Spectroscopy. *Chem. Mater.* **2001**, *13*, 1642–1646. [[CrossRef](#)]
25. Manthiram, A.; Vadivel Murugan, A.; Sarkar, A.; Muraliganth, T. Nanostructured electrode materials for electrochemical energy storage and conversion. *Energy Environ. Sci.* **2008**, *1*, 621–638. [[CrossRef](#)]
26. Kalyani, P.; Kalaiselvi, N. Various aspects of LiNiO_2 chemistry: A review. *Sci. Technol. Adv. Mater.* **2005**, *6*, 689–703. [[CrossRef](#)]
27. Ohzuku, T.; Makimura, Y. Layered Lithium Insertion Material of $\text{LiCo}_{1/3}\text{Ni}_{1/3}\text{Mn}_{1/3}\text{O}_2$ for Lithium-Ion Batteries. *Chem. Lett.* **2001**, *30*, 642–643. [[CrossRef](#)]
28. Ohzuku, T.; Ueda, A.; Nagayama, M. Electrochemistry and Structural Chemistry of LiNiO_2 ($\text{R}3\text{m}$) for 4 Volt Secondary Lithium Cells. *J. Electrochem. Soc.* **1993**, *140*, 1862–1870. [[CrossRef](#)]
29. Myung, S.-T.; Maglia, F.; Park, K.-J.; Yoon, C.S.; Lamp, P.; Kim, S.-J.; Sun, Y.-K. Nickel-Rich Layered Cathode Materials for Automotive Lithium-Ion Batteries: Achievements and Perspectives. *ACS Energy Lett.* **2017**, *2*, 196–223. [[CrossRef](#)]
30. Li, W.; Asl, H.Y.; Xie, Q.; Manthiram, A. Collapse of $\text{LiNi}_{1-x-y}\text{CoxMnyO}_2$ Lattice at Deep Charge Irrespective of Nickel Content in Lithium-Ion Batteries. *J. Am. Chem. Soc.* **2019**, *141*, 5097–5101. [[CrossRef](#)]
31. Ryu, H.-H.; Namkoong, B.; Kim, J.-H.; Belharouak, I.; Yoon, C.S.; Sun, Y.-K. Capacity Fading Mechanisms in Ni-Rich Single-Crystal NCM Cathodes. *ACS Energy Lett.* **2021**, *6*, 2726–2734. [[CrossRef](#)]
32. Lee, Y.S.; Sun, Y.K.; Nahm, K.S. Synthesis and characterization of LiNiO_2 cathode material prepared by an adipic acid-assisted sol-gel method for lithium secondary batteries. *Solid State Ion.* **1999**, *118*, 159–168. [[CrossRef](#)]
33. Croy, J.R.; Long, B.R.; Balasubramanian, M. A path toward cobalt-free lithium-ion cathodes. *J. Power Sources* **2019**, *440*, 227113. [[CrossRef](#)]
34. Alvarado, J.; Wei, C.; Nordlund, D.; Kroll, T.; Sokaras, D.; Tian, Y.; Liu, Y.; Doeff, M.M. Thermal stress-induced charge and structure heterogeneity in emerging cathode materials. *Mater. Today* **2020**, *35*, 87–98. [[CrossRef](#)]
35. Liu, X.; Wu, Z.; Stolarov, S.I.; Denlinger, M.; Masias, A.; Snyder, K. Heat release during thermally-induced failure of a lithium ion battery: Impact of cathode composition. *Fire Saf. J.* **2016**, *85*, 10–22. [[CrossRef](#)]
36. Lei, B.; Zhao, W.; Ziebert, C.; Uhlmann, N.; Rohde, M.; Seifert, H.J. Experimental Analysis of Thermal Runaway in 18,650 Cylindrical Li-Ion Cells Using an Accelerating Rate Calorimeter. *Batteries* **2017**, *3*, 14. [[CrossRef](#)]
37. Jung, R.; Metzger, M.; Maglia, F.; Stinner, C.; Gasteiger, H.A. Oxygen Release and Its Effect on the Cycling Stability of LiNixMnyCozO_2 (NMC) Cathode Materials for Li-Ion Batteries. *J. Electrochem. Soc.* **2017**, *164*, A1361–A1377. [[CrossRef](#)]
38. Kondrakov, A.O.; Schmidt, A.; Xu, J.; Geßwein, H.; Möning, R.; Hartmann, P.; Sommer, H.; Brezesinski, T.; Janek, J. Anisotropic Lattice Strain and Mechanical Degradation of High- and Low-Nickel NCM Cathode Materials for Li-Ion Batteries. *J. Phys. Chem. C* **2017**, *121*, 3286–3294. [[CrossRef](#)]
39. Yan, P.; Zheng, J.; Zhang, J.-G.; Wang, C. Atomic Resolution Structural and Chemical Imaging Revealing the Sequential Migration of Ni, Co, and Mn upon the Battery Cycling of Layered Cathode. *Nano Lett.* **2017**, *17*, 3946–3951. [[CrossRef](#)] [[PubMed](#)]
40. Nam, K.-W.; Yoon, W.-S.; Yang, X.-Q. Structural changes and thermal stability of charged $\text{LiNi}_{1/3}\text{Co}_{1/3}\text{Mn}_{1/3}\text{O}_2$ cathode material for Li-ion batteries studied by time-resolved XRD. *J. Power Sources* **2009**, *189*, 515–518. [[CrossRef](#)]
41. Ghanty, C.; Markovsky, B.; Erickson, E.M.; Talianker, M.; Haik, O.; Tal-Yossef, Y.; Mor, A.; Aurbach, D.; Lampert, J.; Volkov, A.; et al. Li⁺-Ion Extraction/Insertion of Ni-Rich $\text{Li}_{1+x}(\text{NiyCozMnz})\text{wO}_2$ ($0.005 < x < 0.03$; $y:z = 8:1$, $w \approx 1$) Electrodes: In Situ XRD and Raman Spectroscopy Study. *ChemElectroChem* **2015**, *2*, 1479–1486. [[CrossRef](#)]
42. Bak, S.-M.; Hu, E.; Zhou, Y.; Yu, X.; Senanayake, S.D.; Cho, S.-J.; Kim, K.-B.; Chung, K.Y.; Yang, X.-Q.; Nam, K.-W. Structural Changes and Thermal Stability of Charged LiNixMnyCozO_2 Cathode Materials Studied by Combined In Situ Time-Resolved XRD and Mass Spectroscopy. *ACS Appl. Mater. Interfaces* **2014**, *6*, 22594–22601. [[CrossRef](#)]
43. de Biasi, L.; Schwarz, B.; Brezesinski, T.; Hartmann, P.; Janek, J.; Ehrenberg, H. Chemical, Structural, and Electronic Aspects of Formation and Degradation Behavior on Different Length Scales of Ni-Rich NCM and Li-Rich HE-NCM Cathode Materials in Li-Ion Batteries. *Adv. Mater.* **2019**, *31*, 1900985. [[CrossRef](#)] [[PubMed](#)]
44. Renfrew, S.E.; McCloskey, B.D. Residual Lithium Carbonate Predominantly Accounts for First Cycle CO₂ and CO Outgassing of Li-Stoichiometric and Li-Rich Layered Transition-Metal Oxides. *J. Am. Chem. Soc.* **2017**, *139*, 17853–17860. [[CrossRef](#)]
45. Weber, D.; Tripković, Đ.; Kretschmer, K.; Bianchini, M.; Brezesinski, T. Surface Modification Strategies for Improving the Cycling Performance of Ni-Rich Cathode Materials. *Eur. J. Inorg. Chem.* **2020**, *2020*, 3117–3130. [[CrossRef](#)]
46. Li, W.; Dolocan, A.; Oh, P.; Celio, H.; Park, S.; Cho, J.; Manthiram, A. Dynamic behaviour of interphases and its implication on high-energy-density cathode materials in lithium-ion batteries. *Nat. Commun.* **2017**, *8*, 14589. [[CrossRef](#)]
47. Manthiram, A. A reflection on lithium-ion battery cathode chemistry. *Nat. Commun.* **2020**, *11*, 1550. [[CrossRef](#)]

48. Mohan, P.; Kalaignan, G.P. Structure and electrochemical performance of $\text{LiFe}_{x}\text{Ni}_{1-x}\text{O}_2$ ($0.00 \leq x \leq 0.20$) cathode materials for rechargeable lithium-ion batteries. *J. Electroceram.* **2013**, *31*, 210–217. [CrossRef]
49. Wang, D.; Huang, Y.; Huo, Z.; Chen, L. Synthesize and electrochemical characterization of Mg-doped Li-rich layered $\text{Li}[\text{Li}_{0.2}\text{Ni}_{0.2}\text{Mn}_{0.6}]\text{O}_2$ cathode material. *Electrochim. Acta* **2013**, *107*, 461–466. [CrossRef]
50. Dong, X.; Xu, Y.; Xiong, L.; Sun, X.; Zhang, Z. Sodium substitution for partial lithium to significantly enhance the cycling stability of Li_2MnO_3 cathode material. *J. Power Sources* **2013**, *243*, 78–87. [CrossRef]
51. Cormier, M.M.E.; Zhang, N.; Liu, A.; Li, H.; Inglis, J.; Dahn, J.R. Impact of Dopants (Al, Mg, Mn, Co) on the Reactivity of Li_xNiO_2 with the Electrolyte of Li-Ion Batteries. *J. Electrochem. Soc.* **2019**, *166*, A2826–A2833. [CrossRef]
52. Bak, S.-M.; Nam, K.-W.; Chang, W.; Yu, X.; Hu, E.; Hwang, S.; Stach, E.A.; Kim, K.-B.; Chung, K.Y.; Yang, X.-Q. Correlating Structural Changes and Gas Evolution during the Thermal Decomposition of Charged $\text{Li}_x\text{Ni}_{0.8}\text{Co}_{0.15}\text{Al}_{0.05}\text{O}_2$ Cathode Materials. *Chem. Mater.* **2013**, *25*, 337–351. [CrossRef]
53. Dahn, J.R.; Fuller, E.W.; Obrovac, M.; von Sacken, U. Thermal stability of Li_xCoO_2 , Li_xNiO_2 and $\lambda\text{-MnO}_2$ and consequences for the safety of Li-ion cells. *Solid State Ion.* **1994**, *69*, 265–270. [CrossRef]
54. Guilmard, M.; Croguennec, L.; Denux, D.; Delmas, C. Thermal Stability of Lithium Nickel Oxide Derivatives. Part I: $\text{Li}_x\text{Ni}_{1.02}\text{O}_2$ and $\text{Li}_x\text{Ni}_{0.89}\text{Al}_{0.16}\text{O}_2$ ($x = 0.50$ and 0.30). *Chem. Mater.* **2003**, *15*, 4476–4483. [CrossRef]
55. Aishova, A.; Park, G.-T.; Yoon, C.S.; Sun, Y.-K. Cobalt-Free High-Capacity Ni-Rich Layered $\text{Li}[\text{Ni}_{0.9}\text{Mn}_{0.1}]\text{O}_2$ Cathode. *Adv. Energy Mater.* **2020**, *10*, 1903179. [CrossRef]
56. Shirazi Moghadam, Y.; El Kharbachi, A.; Diemant, T.; Melinte, G.; Hu, Y.; Fichtner, M. Toward Better Stability and Reversibility of the $\text{Mn}^{4+}/\text{Mn}^{2+}$ Double Redox Activity in Disordered Rocksalt Oxyfluoride Cathode Materials. *Chem. Mater.* **2021**, *21*, 2334. [CrossRef]
57. Sathiyamoorthi, R.; Manisankar, P.; Shakkthivel, P.; Lee, M.S.; Vasudevan, T. Synthesis, characterization and electrochemical studies of $\text{LiNi}_{0.8}\text{M}_{0.2}\text{O}_2$ cathode material for rechargeable lithium batteries. *Bull. Mater. Sci.* **2008**, *31*, 441–447. [CrossRef]
58. Ohzuku, T.; Ueda, A.; Kouguchi, M. Synthesis and Characterization of $\text{LiAl}_{1/4}\text{Ni}_{3/4}\text{O}_2$ (R 3-m) for Lithium-Ion (Shuttlecock) Batteries. *J. Electrochem. Soc.* **1995**, *142*, 4033–4039. [CrossRef]
59. Li, D.; Peng, Z.; Guo, W.; Yuan, C.; Liu, Y.; Zhou, Y. Synthesis and characterization of $\text{LiNi}_{0.9}\text{Co}_{0.1}\text{O}_2$ for lithium batteries. *J. Mater. Sci.* **2007**, *42*, 9221–9226. [CrossRef]
60. Cheng, X.; Wei, H.; Hao, W.; Li, H.; Si, H.; An, S.; Zhu, W.; Jia, G.; Qiu, X. A Cobalt-Free $\text{Li}(\text{Li}_{0.16}\text{Ni}_{0.19}\text{Fe}_{0.18}\text{Mn}_{0.46})\text{O}_2$ Cathode for Lithium-Ion Batteries with Anionic Redox Reactions. *ChemSusChem* **2019**, *12*, 1162–1168. [CrossRef] [PubMed]
61. Guilmard, M.; Croguennec, L.; Delmas, C. Thermal Stability of Lithium Nickel Oxide Derivatives. Part II: $\text{Li}_x\text{Ni}_{0.70}\text{Co}_{0.15}\text{Al}_{0.15}\text{O}_2$ and $\text{Li}_x\text{Ni}_{0.9}\text{Mn}_{0.10}\text{O}_2$ ($x = 0.50$ and 0.30). Comparison with $\text{Li}_x\text{Ni}_{1.02}\text{O}_2$ and $\text{Li}_x\text{Ni}_{0.89}\text{Al}_{0.16}\text{O}_2$. *Chem. Mater.* **2003**, *15*, 4484–4493. [CrossRef]
62. Bianchini, M.; Fauth, F.; Hartmann, P.; Brezesinski, T.; Janek, J. An in situ structural study on the synthesis and decomposition of LiNiO_2 . *J. Mater. Chem. A* **2020**, *8*, 1808–1820. [CrossRef]
63. Zeng, X.; Jian, T.; Lu, Y.; Yang, L.; Ma, W.; Yang, Y.; Zhu, J.; Huang, C.; Dai, S.; Xi, X. Enhancing High-Temperature and High-Voltage Performances of Single-Crystal $\text{LiNi}_{0.5}\text{Co}_{0.2}\text{Mn}_{0.3}\text{O}_2$ Cathodes through a $\text{LiBO}_2/\text{LiAlO}_2$ Dual-Modification Strategy. *ACS Sustain. Chem. Eng.* **2020**, *8*, 6293–6304. [CrossRef]
64. Li, J.; Li, H.; Stone, W.; Weber, R.; Hy, S.; Dahn, J.R. Synthesis of Single Crystal $\text{LiNi}_{0.5}\text{Mn}_{0.3}\text{Co}_{0.2}\text{O}_2$ for Lithium Ion Batteries. *J. Electrochem. Soc.* **2017**, *164*, A3529–A3537. [CrossRef]
65. Zeng, X.; Zhu, J.; Yang, L.; Zhou, L.; Shao, L.; Hu, S.; Huang, C.; Yang, C.; Qian, D.; Xi, X. Electrochemical stabilities of surface aluminum-doped $\text{LiNi}_{0.5}\text{Co}_{0.2}\text{Mn}_{0.3}\text{O}_2$ single crystals under different cutoff voltages. *J. Electroanal. Chem.* **2019**, *838*, 94–100. [CrossRef]
66. Lu, S.; Liu, Y.; He, Z.; Li, Y.; Zheng, J.; Mao, J.; Dai, K. Synthesis and properties of single-crystal Ni-rich cathode materials in Li-ion batteries. *Trans. Nonferrous Met. Soc. China* **2021**, *31*, 1074–1086. [CrossRef]
67. Li, J.; Cameron, A.R.; Li, H.; Glazier, S.; Xiong, D.; Chatzidakis, M.; Allen, J.; Botton, G.A.; Dahn, J.R. Comparison of Single Crystal and Polycrystalline $\text{LiNi}_{0.5}\text{Mn}_{0.3}\text{Co}_{0.2}\text{O}_2$ Positive Electrode Materials for High Voltage Li-Ion Cells. *J. Electrochem. Soc.* **2017**, *164*, A1534–A1544. [CrossRef]
68. Wang, C.; Yu, R.; Hwang, S.; Liang, J.; Li, X.; Zhao, C.; Sun, Y.; Wang, J.; Holmes, N.; Li, R.; et al. Single crystal cathodes enabling high-performance all-solid-state lithium-ion batteries. *Energy Storage Mater.* **2020**, *30*, 98–103. [CrossRef]
69. Xiong, C.; Liu, F.; Gao, J.; Jiang, X. One-Spot Facile Synthesis of Single-Crystal $\text{LiNi}_{0.5}\text{Co}_{0.2}\text{Mn}_{0.3}\text{O}_2$ Cathode Materials for Li-ion Batteries. *ACS Omega* **2020**, *5*, 30356–30362. [CrossRef] [PubMed]
70. Li, Y.; Wu, C.; Bai, Y.; Liu, L.; Wang, H.; Wu, F.; Zhang, N.; Zou, Y. Hierarchical Mesoporous Lithium-Rich $\text{Li}[\text{Li}_{0.2}\text{Ni}_{0.2}\text{Mn}_{0.6}]\text{O}_2$ Cathode Material Synthesized via Ice Templating for Lithium-Ion Battery. *ACS Appl. Mater. Interfaces* **2016**, *8*, 18832–18840. [CrossRef] [PubMed]
71. Pan, H.; Zhang, S.; Chen, J.; Gao, M.; Liu, Y.; Zhu, T.; Jiang, Y. Li- and Mn-rich layered oxide cathode materials for lithium-ion batteries: A review from fundamentals to research progress and applications. *Mol. Syst. Des. Eng.* **2018**, *3*, 748–803. [CrossRef]
72. Chong, S.; Wu, Y.; Chen, Y.; Shu, C.; Liu, Y. A strategy of constructing spherical core-shell structure of $\text{Li}_{1.2}\text{Ni}_{0.2}\text{Mn}_{0.6}\text{O}_2@\text{Li}_{1.2}\text{Ni}_{0.4}\text{Mn}_{0.4}\text{O}_2$ cathode material for high-performance lithium-ion batteries. *J. Power Sources* **2017**, *356*, 153–162. [CrossRef]
73. Jun, D.-W.; Yoon, C.S.; Kim, U.-H.; Sun, Y.-K. High-Energy Density Core–Shell Structured $\text{Li}[\text{Ni}_{0.95}\text{Co}_{0.025}\text{Mn}_{0.025}]\text{O}_2$ Cathode for Lithium-Ion Batteries. *Chem. Mater.* **2017**, *29*, 5048–5052. [CrossRef]

74. Ran, Q.; Zhao, H.; Hu, Y.; Hao, S.; Liu, J.; Li, H.; Liu, X. Enhancing surface stability of $\text{LiNi}_{0.8}\text{Co}_{0.1}\text{Mn}_{0.1}\text{O}_2$ cathode with hybrid core-shell nanostructure induced by high-valent titanium ions for Li-ion batteries at high cut-off voltage. *J. Alloys Compd.* **2020**, *834*, 155099. [[CrossRef](#)]
75. Hou, P.; Zhang, H.; Zi, Z.; Zhang, L.; Xu, X. Core–shell and concentration-gradient cathodes prepared via co-precipitation reaction for advanced lithium-ion batteries. *J. Mater. Chem. A* **2017**, *5*, 4254–4279. [[CrossRef](#)]
76. Zhang, N.; Zaker, N.; Li, H.; Liu, A.; Inglis, J.; Jing, L.; Li, J.; Li, Y.; Botton, G.A.; Dahn, J.R. Cobalt-Free Nickel-Rich Positive Electrode Materials with a Core–Shell Structure. *Chem. Mater.* **2019**, *31*, 10150–10160. [[CrossRef](#)]
77. Sun, Y.-K.; Chen, Z.; Noh, H.-J.; Lee, D.-J.; Jung, H.-G.; Ren, Y.; Wang, S.; Yoon, C.S.; Myung, S.-T.; Amine, K. Nanostructured high-energy cathode materials for advanced lithium batteries. *Nat. Mater.* **2012**, *11*, 942–947. [[CrossRef](#)]
78. Hua, W.; Schwarz, B.; Azmi, R.; Müller, M.; Dewi Darma, M.S.; Knapp, M.; Senyshyn, A.; Heere, M.; Missyul, A.; Simonelli, L.; et al. Lithium-ion (de)intercalation mechanism in core-shell layered $\text{Li}(\text{Ni},\text{Co},\text{Mn})\text{O}_2$ cathode materials. *Nano Energy* **2020**, *78*, 105231. [[CrossRef](#)]
79. Wang, E.; Shao, C.; Qiu, S.; Chu, H.; Zou, Y.; Xiang, C.; Xu, F.; Sun, L. Organic carbon gel assisted-synthesis of $\text{Li}_{1.2}\text{Mn}_{0.6}\text{Ni}_{0.2}\text{O}_2$ for a high-performance cathode material for Li-ion batteries. *RSC Adv.* **2017**, *7*, 1561–1566. [[CrossRef](#)]
80. Li, Y.; Bai, Y.; Bi, X.; Qian, J.; Ma, L.; Tian, J.; Wu, C.; Wu, F.; Lu, J.; Amine, K. An Effectively Activated Hierarchical Nano-/Microspherical $\text{Li}_{1.2}\text{Ni}_{0.2}\text{Mn}_{0.6}\text{O}_2$ Cathode for Long-Life and High-Rate Lithium-Ion Batteries. *ChemSusChem* **2016**, *9*, 728–735. [[CrossRef](#)] [[PubMed](#)]
81. de Boisse, B.M.; Jang, J.; Okubo, M.; Yamada, A. Cobalt-Free O_2 -Type Lithium-Rich Layered Oxides. *J. Electrochem. Soc.* **2018**, *165*, A3630–A3633. [[CrossRef](#)]
82. Qu, X.; Yu, Z.; Ruan, D.; Dou, A.; Su, M.; Zhou, Y.; Liu, Y.; Chu, D. Enhanced Electrochemical Performance of Ni-Rich Cathode Materials with $\text{Li}_{1.3}\text{Al}_{0.3}\text{Ti}_{1.7}(\text{PO}_4)_3$ Coating. *ACS Sustain. Chem. Eng.* **2020**, *8*, 5819–5830. [[CrossRef](#)]
83. Neudeck, S.; Mazilkin, A.; Reitz, C.; Hartmann, P.; Janek, J.; Brezesinski, T. Effect of Low-Temperature Al_2O_3 ALD Coating on Ni-Rich Layered Oxide Composite Cathode on the Long-Term Cycling Performance of Lithium-Ion Batteries. *Sci. Rep.* **2019**, *9*, 5328. [[CrossRef](#)] [[PubMed](#)]
84. Xu, C.; Xiang, W.; Wu, Z.; Xu, Y.; Li, Y.; Wang, Y.; Xiao, Y.; Guo, X.; Zhong, B. Highly Stabilized Ni-Rich Cathode Material with Mo Induced Epitaxially Grown Nanostructured Hybrid Surface for High-Performance Lithium-Ion Batteries. *ACS Appl. Mater. Interfaces* **2019**, *11*, 16629–16638. [[CrossRef](#)] [[PubMed](#)]
85. Yan, P.; Zheng, J.; Liu, J.; Wang, B.; Cheng, X.; Zhang, Y.; Sun, X.; Wang, C.; Zhang, J.-G. Tailoring grain boundary structures and chemistry of Ni-rich layered cathodes for enhanced cycle stability of lithium-ion batteries. *Nat. Energy* **2018**, *3*, 600–605. [[CrossRef](#)]
86. Schipper, F.; Bouzaglo, H.; Dixit, M.; Erickson, E.M.; Weigel, T.; Taliander, M.; Grinblat, J.; Burstein, L.; Schmidt, M.; Lampert, J.; et al. From Surface ZrO_2 Coating to Bulk Zr Doping by High Temperature Annealing of Nickel-Rich Lithiated Oxides and Their Enhanced Electrochemical Performance in Lithium Ion Batteries. *Adv. Energy Mater.* **2018**, *8*, 1701682. [[CrossRef](#)]
87. Cheng, X.; Zheng, J.; Lu, J.; Li, Y.; Yan, P.; Zhang, Y. Realizing superior cycling stability of Ni-Rich layered cathode by combination of grain boundary engineering and surface coating. *Nano Energy* **2019**, *62*, 30–37. [[CrossRef](#)]
88. Sun, H.H.; Ryu, H.-H.; Kim, U.-H.; Weeks, J.A.; Heller, A.; Sun, Y.-K.; Mullins, C.B. Beyond Doping and Coating: Prospective Strategies for Stable High-Capacity Layered Ni-Rich Cathodes. *ACS Energy Lett.* **2020**, *5*, 1136–1146. [[CrossRef](#)]
89. Zhang, Q.; Bruck, A.M.; Stavola, A.M.; Liang, W.; Aurora, P.; Gallaway, J.W. Enhanced Electrochemical Stability of Sulfide-Based $\text{LiNi}_{0.8}\text{Mn}_{0.1}\text{Co}_{0.1}\text{O}_2$ All-Solid-State Batteries by Ti Surface Doping. *Batter. Supercaps* **2021**, *4*, 529–535. [[CrossRef](#)]
90. Wu, F.; Xue, Q.; Li, L.; Zhang, X.; Huang, Y.; Fan, E.; Chen, R. The positive role of $(\text{NH}_4)_3\text{AlF}_6$ coating on $\text{Li}[\text{Li}_{0.2}\text{Ni}_{0.2}\text{Mn}_{0.6}]\text{O}_2$ oxide as the cathode material for lithium-ion batteries. *RSC Adv.* **2017**, *7*, 1191–1199. [[CrossRef](#)]
91. Zhang, H.Z.; Qiao, Q.Q.; Li, G.R.; Ye, S.H.; Gao, X.P. Surface nitridation of Li-rich layered $\text{Li}(\text{Li}_{0.17}\text{Ni}_{0.25}\text{Mn}_{0.58})\text{O}_2$ oxide as cathode material for lithium-ion battery. *J. Mater. Chem.* **2012**, *22*, 13104–13109. [[CrossRef](#)]
92. Chong, S.; Chen, Y.; Yan, W.; Guo, S.; Tan, Q.; Wu, Y.; Jiang, T.; Liu, Y. Suppressing capacity fading and voltage decay of Li-rich layered cathode material by a surface nano-protective layer of CoF_2 for lithium-ion batteries. *J. Power Sources* **2016**, *332*, 230–239. [[CrossRef](#)]
93. Ho, V.-C.; Jeong, S.; Yim, T.; Mun, J. Crucial role of thioacetamide for ZrO_2 coating on the fragile surface of Ni-rich layered cathode in lithium ion batteries. *J. Power Sources* **2020**, *450*, 227625. [[CrossRef](#)]
94. Ming, Y.; Xiang, W.; Qiu, L.; Hua, W.-B.; Li, R.; Wu, Z.-G.; Xu, C.-L.; Li, Y.-C.; Wang, D.; Chen, Y.-X.; et al. Dual Elements Coupling Effect Induced Modification from the Surface into the Bulk Lattice for Ni-Rich Cathodes with Suppressed Capacity and Voltage Decay. *ACS Appl. Mater. Interfaces* **2020**, *12*, 8146–8156. [[CrossRef](#)]
95. Deng, T.; Fan, X.; Cao, L.; Chen, J.; Hou, S.; Ji, X.; Chen, L.; Li, S.; Zhou, X.; Hu, E.; et al. Designing In-Situ-Formed Interphases Enables Highly Reversible Cobalt-Free LiNiO_2 Cathode for Li-ion and Li-metal Batteries. *Joule* **2019**, *3*, 2550–2564. [[CrossRef](#)]
96. Li, W.; Lee, S.; Manthiram, A. High-Nickel NMA: A Cobalt-Free Alternative to NMC and NCA Cathodes for Lithium-Ion Batteries. *Adv. Mater.* **2020**, *32*, 2002718. [[CrossRef](#)]
97. Seo, J.H.; Kim, U.-H.; Sun, Y.-K.; Yoon, C.S. Multi-Doped (Ga,B) $\text{Li}[\text{Ni}_{0.885}\text{Co}_{0.100}\text{Al}_{0.015}]\text{O}_2$ Cathode. *J. Electrochem. Soc.* **2020**, *167*, 100557. [[CrossRef](#)]
98. Park, K.-J.; Choi, M.-J.; Maglia, F.; Kim, S.-J.; Kim, K.-H.; Yoon, C.S.; Sun, Y.-K. High-Capacity Concentration Gradient $\text{Li}[\text{Ni}_{0.865}\text{Co}_{0.120}\text{Al}_{0.015}]\text{O}_2$ Cathode for Lithium-Ion Batteries. *Adv. Energy Mater.* **2018**, *8*, 1703612. [[CrossRef](#)]

99. Kim, U.-H.; Kuo, L.-Y.; Kaghazchi, P.; Yoon, C.S.; Sun, Y.-K. Quaternary Layered Ni-Rich NCMA Cathode for Lithium-Ion Batteries. *ACS Energy Lett.* **2019**, *4*, 576–582. [[CrossRef](#)]
100. Yoon, C.S.; Park, K.-J.; Kim, U.-H.; Kang, K.H.; Ryu, H.-H.; Sun, Y.-K. High-Energy Ni-Rich Li[Ni_xCo_yMn_{1-x-y}]O₂ Cathodes via Compositional Partitioning for Next-Generation Electric Vehicles. *Chem. Mater.* **2017**, *29*, 10436–10445. [[CrossRef](#)]
101. Lim, B.-B.; Myung, S.-T.; Yoon, C.S.; Sun, Y.-K. Comparative Study of Ni-Rich Layered Cathodes for Rechargeable Lithium Batteries: Li[Ni_{0.85}Co_{0.11}Al_{0.04}]O₂ and Li[Ni_{0.84}Co_{0.06}Mn_{0.09}Al_{0.01}]O₂ with Two-Step Full Concentration Gradients. *ACS Energy Lett.* **2016**, *1*, 283–289. [[CrossRef](#)]
102. Sun, Y.-K.; Myung, S.-T.; Kim, M.-H.; Prakash, J.; Amine, K. Synthesis and Characterization of Li[(Ni₂0.8Co_{0.1}Mn₂0.1)_{0.8}(Ni_{0.5}Mn_{0.5})_{0.2}]O₂ with the Microscale Core–Shell Structure as the Positive Electrode Material for Lithium Batteries. *J. Am. Chem. Soc.* **2005**, *127*, 13411–13418. [[CrossRef](#)]
103. Kim, U.-H.; Kim, J.-H.; Hwang, J.-Y.; Ryu, H.-H.; Yoon, C.S.; Sun, Y.-K. Compositionally and structurally redesigned high-energy Ni-rich layered cathode for next-generation lithium batteries. *Mater. Today* **2019**, *23*, 26–36. [[CrossRef](#)]
104. Kim, U.-H.; Ryu, H.-H.; Kim, J.-H.; Mücke, R.; Kaghazchi, P.; Yoon, C.S.; Sun, Y.-K. Microstructure-Controlled Ni-Rich Cathode Material by Microscale Compositional Partition for Next-Generation Electric Vehicles. *Adv. Energy Mater.* **2019**, *9*, 1803902. [[CrossRef](#)]
105. Yoon, C.S.; Jun, D.-W.; Myung, S.-T.; Sun, Y.-K. Structural Stability of LiNiO₂ Cycled above 4.2 V. *ACS Energy Lett.* **2017**, *2*, 1150–1155. [[CrossRef](#)]
106. Ryu, H.-H.; Park, G.-T.; Yoon, C.S.; Sun, Y.-K. Suppressing detrimental phase transitions via tungsten doping of LiNiO₂ cathode for next-generation lithium-ion batteries. *J. Mater. Chem. A* **2019**, *7*, 18580–18588. [[CrossRef](#)]
107. Ma, R.; Zhao, Z.; Fu, J.; Lv, H.; Li, C.; Wu, B.; Mu, D.; Wu, F. Tuning Cobalt-Free Nickel-Rich Layered LiNi_{0.9}Mn_{0.1}O₂ Cathode Material for Lithium-Ion Batteries. *ChemElectroChem* **2020**, *7*, 2637–2642. [[CrossRef](#)]